Photon Splitting in Different Astrophysical Conditions

Bachelor Thesis

for obtainment of the academical degree

Bachelor of Science

(B.Sc.)

at the University of Siegen

Department Physik

submitted by

Philip Rühl

December 2013

Contents

1 Introduction

1.1 Cosmic Rays

The cosmos has always been an object of scientific interest since the beginnings of civilisation. It has been investigated by an innumerable amount of scientists and in many different ways, reaching from simple observations of the luminaries without any devices to analysis of exotic phenomena like the existence of dark matter or gravitation waves radiated by binary star systems formed by white dwarfs. Despite the cosmos is likely to be the most considered object in the history of science, there are still many mysterious phenomena which are not understood even in modern physics. The main difficulty within researches in terms of astrophysics are the large dimensions one has to deal with and the comparatively small stream of available information provided by the boundary conditions of the Earth, which offers a very restricted space for observations. This stream of information is basically represented by various kinds of radiation like disengaged massive particles or electromagnetic waves at all kinds of wavelength. Making astrophysical observations using extraterrestrial particles is a comparatively young method discovered in the second decade of the 20th century, where, at the first time, natural ionizing radiation could be related to outer space. This special kind of ionizing radiation was named cosmic rays.

First hints to extraterrestrial radiation where discovered in the beginning of the 20th century. By analysing the effect, that isolated electrometers are discharged continuously it has been figured out that there is an omnipresent radioactivity in nature. With Theodor Wulf (1910) measuring the dependence of the radiation intensity on the altitude by taking data at the top of the Eiffel Tower, the sources of that radiation were determined to originate somewhere in the ground. Further analyses of that terrestrial radiation induced by radioactive ores where done by Victor Hess (1912), who measured the decrease of radiation intensity with further rising altitude. Therefore he went for a couple of balloon flights which made measurements in altitudes up to 17.500 feet possible. In the first place the intensity decreased, as expected, which proofed, that the major part of the natural ionizing radiation on the Earth's surface came from the ground. However, with rising altitude, the intensity started to increase again up to ten times of the prior intensity

on the ground. This was a hint for the fact, that these radiations did not originate from the ground but from some extraterrestrial sources. For the measurements gave the same results in the night as on the day, one could conclude, that the radiation had to originate from somewhere outside of the solar system.

In 1938, the researches of Pierre Auger in the field of cosmic radiation have shown, that the extraterrestrial radiation can not be measured directly on Earth since the primary particles interact with the matter of the atmosphere and therefore initiate cascades of particles. Such cascades of secondary particles are nowadays known as extensive air showers. Pierre Auger made this discovery when he took measurements from an array of detectors, which were arranged with spaces of 300m next to each other. It turned out, that always bunches of particles arrived at the same time at adjacent detectors, which means that they had to belong to the same air shower initiated by one primary particle. Consequently the energy of the primary particles had to be much higher then primarily assumed. Nowadays, the highest measured particle energies are even above 10^{20}eV, known as ultra high energy cosmic rays (UHECR). An all-particle spectrum of the cosmic ray flux measured by different experiments is shown in figure 1 (see [13]).

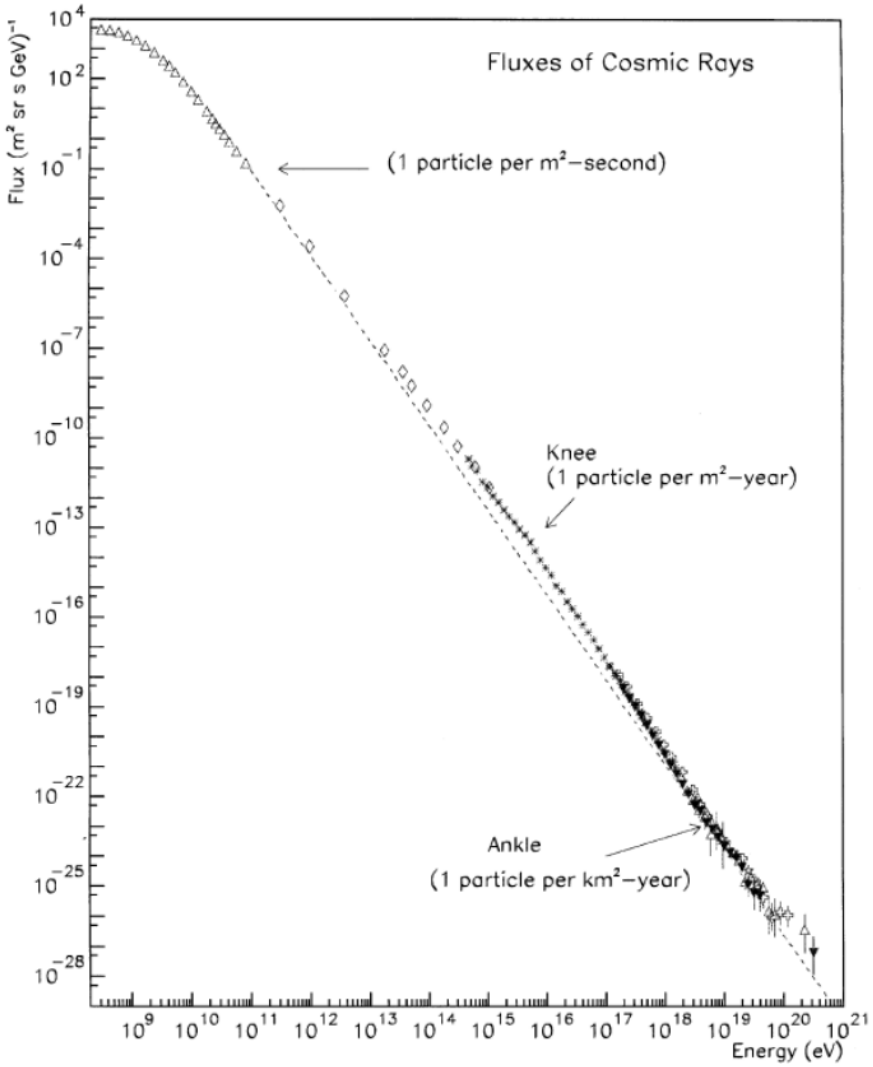

Figure 1: The flux of cosmic ray particles from the GeV range up to UHECR ($\sim 10^{20} eV$). The changing power laws at the "knee" and the "ankle" give hints to different accelerating mechanisms. The sudden cutoff of the spectrum at energies above 10^{20}eV could be explained by the GZK-effect [15],[16]. (figure taken from [13])

1.2 Unsettled Questions

To understand the Universe as a whole, it is necessary to analyse and understand every information that can somehow be received from the cosmos. For every kind of cosmic radiation carries its own bunch of information like its origin or its creation as well as its acceleration

mechanism one has to research the whole spectrum of cosmic rays to investigate every achievable information. Despie the discovery of cosmic rays was about one hundred years ago, there are still many unsettled questions about it. One big question is about the sources of the highest energy particles and their accelerating mechanisms. As possible sources, one could imagine extremely high and rapidly changing magnetic fields as they occur within pulsars and active galactic nuclei. There are evidences, but no experimental proof yet, that such point sources are really existing. In addition to that, the composition of particle types arriving at Earth also is not known precisely by now. For the particle type would give a hint to the accelerating mechanism and therefore also to the possible sources and the prevailing magnetic fields in the Universe, these questions are closely related to each other. There are some big experiments running which deal with the question of the particle composition at the top of the energy scale like the Telescope Array [17] Project and the Pierre Auger Observatory [19], which is specialized to identify the most energetic particles in the flux of cosmic rays. The highest energy particle observed so far, known as the "Fly's Eye event", was at $3.2 \cdot 10^{20}$eV, measured by the HiRes Fly's Eye experiment [18]. The current experimental status concerning the particle composition differs within the different experiments. Most experiments see tendencies towards a major part of protons at the highest energies whereas the Auger Observatory claims to see a larger part of heavy nuclei instead of protons. In case there is a large part of protons in the flux of highest energy particles, there would also be a significant fraction of photons and neutrinos expected at energies of $10^{18} - 10^{19}$eV due to the CZK-effect, which predicts a rapid decrease of the proton flux on Earth at 5×10^{19}eV. This decrease is because of the interactions of the protons with the cosmic microwave background, in which charged and neutral pions are produced ($p_{GZK} + \gamma_{CMB} \rightarrow \Delta^+ \rightarrow \pi^0 + p$; $p_{GZK} + \gamma_{CMB} \rightarrow \Delta^+ \rightarrow \pi^+ + n$), which most likely decay to photons and neutrinos. These particles are expected are predicted by models including the GZK-effect, but have not yet been identidied in the available observational data.

1.3 UHE Photons

Besides the GZK-effect, there are other possible reasons for a fraction of photons among the highest energy cosmic rays. In the broadest sense there are two kinds of models, which pre-

dict ultra high energy (UHE) photons. In the more conservative acceleration models, diverse primary charged particles are claimed to start with low energies and then being accelerated by very strong electric fields or rapidly changing magnetic fields, like they occur at neutron stars or active galactic nuclei. In most of the acceleration models, an UHE photon is emitted during the decay of a neutral pion previously produced by a charged primary particle at an extreme high energy interacting with the cosmic microwave background. UHE photons can also be emitted by a primary proton radiating bremsstrahlung while crossing magnetic fields. These models predict, that there are low fractions photons at energies above 10^{19}eV in case the most energetic particles were identified as protons. The other way round, a detection of primary UHE photons could give a hint towards protons at the highest energies.

The other type of models, the so called non-acceleration models, declare more exotic scenarios like annihilation of topological defects, decay of super heavy dark matter particles or the Z-burst scenario [1] as the sources for UHE photons. They predict a large fraction of photons and neutrinos at extreme high energies above the GZK-limit. The different predictions of photon and neutrino fluxes at the highest energies make it very important to search for those particles in order to distinguish between the models.

Currently, the highest observed energies, which can be related to photons, are at 10^{14}eV [1], which is quite remarkable because at these energies, the average propagation length has a minimum ($\sim$ 3kpc) [1] due to a maximum in the cross section for interactions with the cosmic microwave background. That means that the sources of these particles have to be somewhere within our galaxy. With higher photon energies the cross section decreases again, so that propagation lenghts up to 100Mpc are expected which gives a larger territory for possible sources. The particle composition at the highest energies is still very unclear. That there is actually a chance for photons to exist among the highest energy particles, which are detected, one can see by comparing the current simulations for instance with the Fly's Eye particle. By doing this, one finds a 1.5σ discrepancy of the simulations to the measurement data [2]. Even though the simulations for protons and iron are closer to the measurement data, photon candidates can not be ruled out.

1.4 Importance of Considering Magnetic Preshowers

Because the cosmic primary particles above 10^{15}eV cannot be measured directly, one has to interpret all available observables to identify the particles from air showers initiated at the top of the atmosphere (t.o.a.) and measured during their propagation and hitting the ground. Obviously one of the requirements for correct interpretation of the measurement data is a useful model for the propagation of air showers in the atmosphere. Therefore, every single effect, which can happen during the air shower propagation has to be taken into account. Otherwise, the data, measured on the ground, would be misinterpreted and yield a wrong picture of the primary particles properties or even its type. Very precise models of extensive air shower propagations have already been developed and used in air shower simulation programs like CORSIKA [20],[21] or Aires [22]. Unlike for protons or heavy nuclei, there exists a chance for primary photons to interact with the field quantums of the geomagnetic field. This effect is negligible at low energies, but becomes highly significant at photon energies at about 10^{19}eV. When a photon interacts with the magnetic field, an electron-positron pair could be created, which produces further photons due to bremsstrahlung. This initial particle cascading is known as magnetic preshowers [3]. These electromagnetic particle cascades can already begin in the magnetosphere far above the Earth's atmosphere and effectively deform the shape of the air showers one can measure on Earth. Therefore, neglecting the preshower effect would falsify the reconstruction of an air shower. For instance, the value for the atmospheric depth X_{max} at which a photon air shower of extremely large energy reaches its maximum size would be overestimated if preshowers were neglected [2]. In case the preshower occurs, the shape of photon induced air showers does not just depend on the primary energies but also on the geographical position of the observation and the arrival directions of the primary particles. This is because the cross section of the preshower effect depends on the component of the magnetic field transverse to the particle momentum.
For simulating such preshower effects, the PRESHOWER program has been developed [3]. It can be used as an independent program or as a module of CORSIKA. By now, PRESHOWER takes the effect of magnetic pair production and electron bremsstrahlung into account. As an example, in Fig. 2, the energy spectrum of all preshower particles at t.o.a. considering 500 primary photons at 10^{20}eV has been simulated with PRESHOWER and plotted in a histogram.

In this plot, the two types of particles, i.e. photons and electrons, are distinguished in separate histograms.

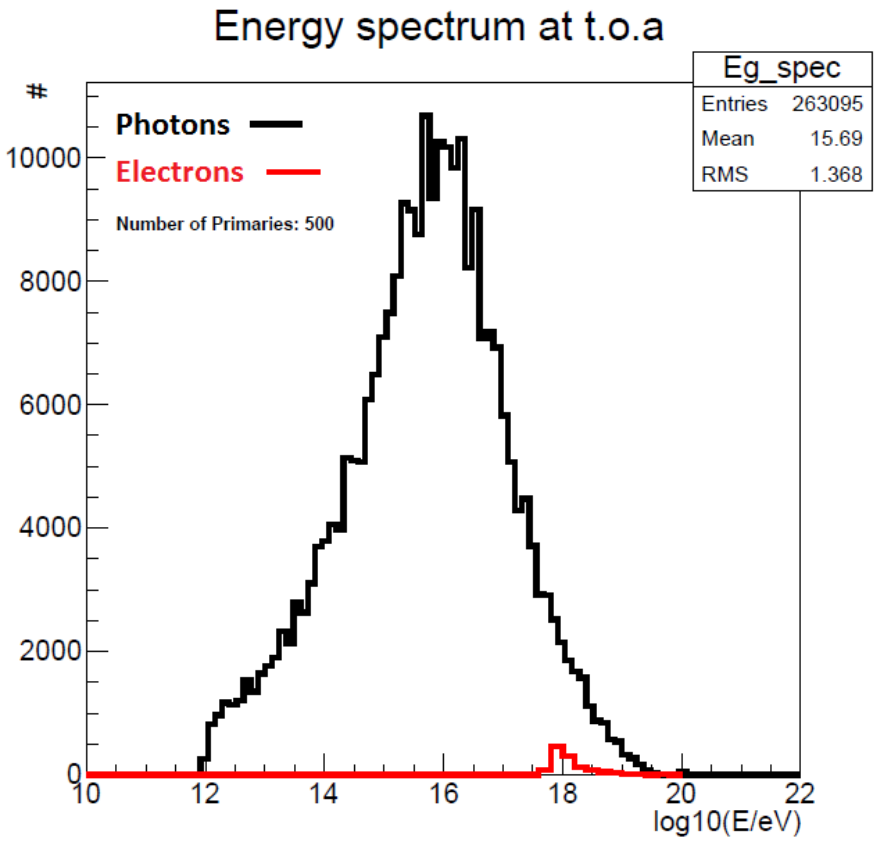

Figure 2: A simulation of the energy and particle distribution at the top of the atmosphere considering the effects of magnetic pair production. Number of primary photons: 650; zenith angle: 60°; azimuth angle: 180° counterclockwise from geographical north; energy of primary photon: 10^{20}eV; top of atmosphere: 112.83km; geographical position of observatory, longitude: −69.2°, latitude: −35.2°; year of simulated observation: 2013

One can see, that a discrete spectrum of primary energies leads to an energy distribution extending over many orders of magnitude at the t.o.a.. The maximum in this case is about four orders of magnitude lower then the primary energies. One can also see a small but significant peak at 10^{20}eV, which refers to a few photons which did not interact during their whole way through the magnetosphere. Hence, that figure 2 is just one example for a possible observation.

The spectrum changes dramatically when varying the arrival direction of the photons, their energy or the coordinates of the observatory. Here the location of the Pierre Auger observatory. Also the year of observation might change the results because of the dynamic nature of the Earth's magnetic field, simulated with the IGRF model, which is used in PRESHOWER.
Pair production is not the only interaction photons can undergo when travelling through a magnetic field. For certain conditions there could exist a non negligible probability of a photon to split in two lower energy photons. This effect has not been includet neither in the PRESHOWER program nor in any other public preshower code. Now, the question arises, whether photon splitting plays an important role within the development of preshowers on Earth and, considering the applications of PRESHOWER to other astrophysical circumstances, under which condition in general photon splitting could occur. In the following sections the photon splitting effect shall be analysed under various conditions and tested in terms of its relative significance compared to pair production (section 2.4) and its absolute significance (section 2.5).

2 Analysis

2.1 Tools Used for Calculations and Plottings

Both photon splitting and pair production calculations were performed within the PRESHOWER frame. The basic structure of the program, written in the language C, has been modified to calculate the values relevent for the two-dimensional plots shown in figures 5, 6, 8, 9, 11, 12 and 13. Although it would have been possible to write a program for itself to calculate these values, it was convenient to modify the code of PRESHOWER because the calculation of the attenuation coefficient α for pair production is already implemented there. Moreover, depending on the results of the research, the photon splitting attenuation coefficient could be implemented into the program anyway.
To calculate the integral representations of the $\mathscr{C}$-coefficient as used in eq. 2, a very high precision of the float-variables was needed. For the maximal precision of the standard variables in C, as given by a long double, has just 20 digits of precision, an alternative program, called Genius Math Tool [4], was used for these calculations. With this program it was possible, to access

an arbitrary precision, which was just limited by the capacity of the CPUs cache memory. The precision at this point was set to 2048 Bits, i.e. ≈ 600 digits. For adding $\mathscr{C}$ to PRESHOWER, a table of numerically calculated values has been generated and implemented as a function, which interpolates the numerical values with power laws. This has been acieved by using linear interpolations between nearby points while drawing both, the x- and the y-axis in logarithmic scales. Alternatively, the arbitrary precision could be achieved by using the gnu multiple precision arithmetic (gmp) library for C/C++ [5].
All shown plots were made by using ROOT [6] to read and process the output data files generated by the programs mentioned above.

2.2 Photon Splitting

As mentioned earlier, besides magnetic pair production, there is another effect, called photon splitting ($\gamma \rightarrow \gamma\gamma$), that can happen to a photon travelling through an ambient megnetic field. That means, that there is a chance for a single primary photon to split into two secondary photons in the environment of a quantum of the magnetic field. The photon splitting effect is a third order QED process which can effectively occur at certain photon energies and magnetic field strengths. Neglecting the the low energy photon from the magnetic field, the simplified Feynman Diagram of photon splitting in the leading order is a triangular diagram as shown in figure 3.

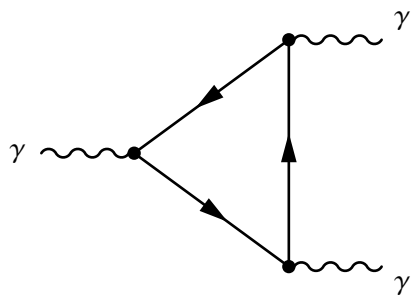

Figure 3: Triangular Feynman diagram for photon splitting (without the photon from the magnetic field)

For this effect, being an attenuation process for electromagnetic radiation, the attenuation coefficient [1] has been calculated in detail by Stoneham [7] using the electron propagator of a constant ambient magnetic field derived by Géhéniau (1950) and Géhéniau and Demeur (1951).
In the limit of no dispersion, i.e.

$$\frac{B}{B_{cr}}\frac{E_\gamma}{m_e c^2} \lesssim 1, \tag{1}$$

the attenuation coefficient δ, averaged over all polarisation states, can be written as a function of the photon energy and the magnetic field strength:

$$\delta_{sk}(B, E_\gamma) = \frac{\alpha_{em}^3}{10\pi^2}\frac{1}{\lambda\!\!\!^{-}}\left(\frac{19}{315}\right)^2 B'^6 \mathscr{C}(B')\left(\frac{E_\gamma}{m_e c^2}\right)^5 \sin^6(\theta_{kB}) \tag{2}$$

where α_{em} is the fine structure constant, $\lambda\!\!\!^{-} = \hbar/(m_e c)$ is the reduced Compton wavelength, θ_{kB} is the angle between the momentum of the photon and the direction of the magnetic field and $B' = B/B_{cr}$ denotes the relative magnetic field to the critical field strength $B_{cr} = (m_e^2 c^3)/(e\hbar) \approx 4.413 \cdot 10^{13}$G.

The $\mathscr{C}$-coefficient can be represented by:

$$\mathscr{C}(B') = \frac{1}{12}\left(\frac{315}{19}\right)^2 (3M_1^2 + M_2^2) \tag{3}$$

where M_1 and M_2 can be expressed by the following integral representations:

$$\begin{aligned} M_1 &= \frac{1}{B'^4}\int_0^\infty ds \frac{e^{-s/B'}}{s}\left[\left(-\frac{3}{4s}+\frac{s}{6}\right)\frac{\cosh s}{\sinh s} + \frac{3+2s^2}{12\sinh^2 s} + \frac{s\cosh s}{2\sinh^3 s}\right]; \\ M_2 &= \frac{1}{B'^4}\int_0^\infty ds \frac{e^{-s/B'}}{s}\left(\frac{3}{4s}\frac{\cosh s}{\sinh s} + \frac{3-4s^2}{4\sinh^2 s} - \frac{3s^2}{2\sinh^4 s}\right) \end{aligned} \tag{4}$$

The numerical solutions for $\mathscr{C}$, M_1 and M_2 have been visualized in figure 4.

[1] The attenuation coefficient is defined as the inverse of the photon path length in a constant magnetic field after which the probability, that the photon has not underwent splitting has dropped to 1/e, where e is the Euler's number.

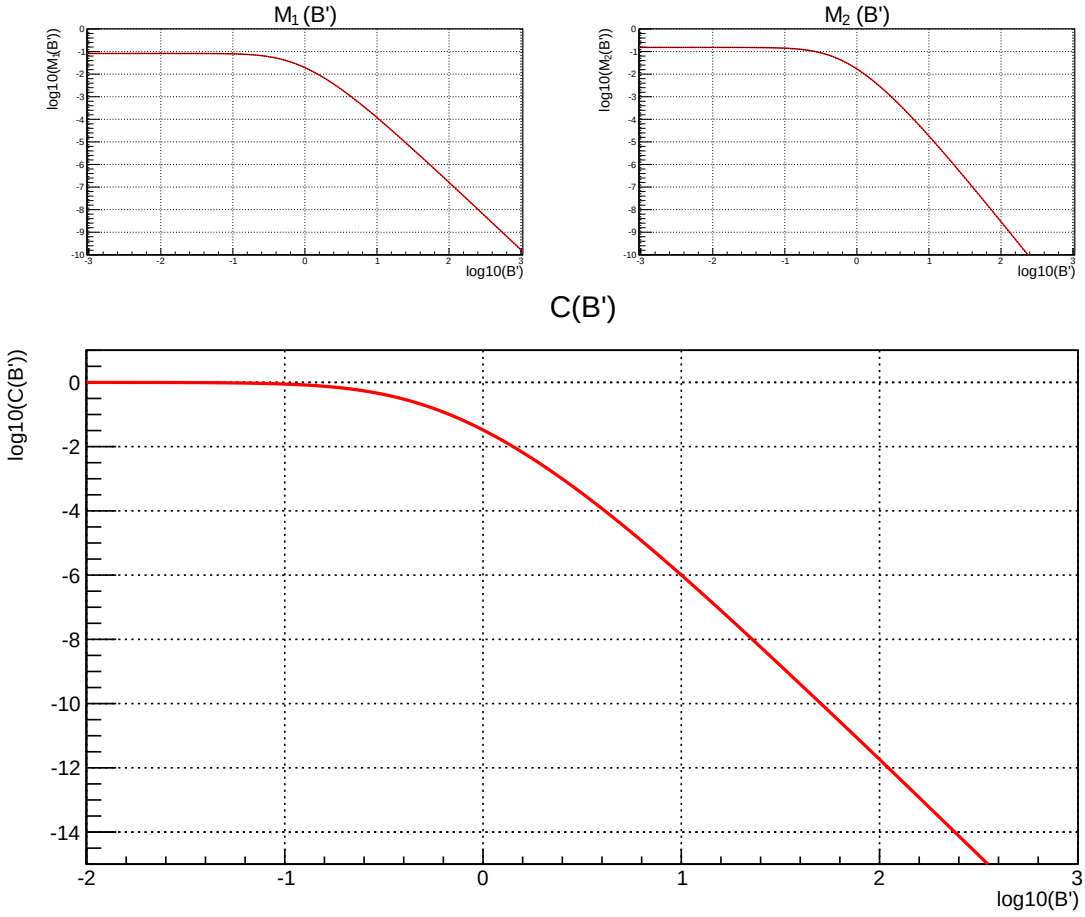

Figure 4: The M_1- and the M_2-coefficients (upper panels) and the $\mathscr{C}$-coefficient (lower panel) as functions of $B'(= B/B_{cr})$

According to Stoneham [7], the limits for M_1 and M_2, as B' goes to zero, are

$$\begin{aligned} M_1(B') &\xrightarrow{B'\to 0} \frac{26}{315}, \\ M_2(B') &\xrightarrow{B'\to 0} \frac{48}{315}, \end{aligned} \tag{5}$$

and, according to Harding and Barring [9], as $B \gg B_{cr}$, the M_1- and M_2-coefficients behave like power laws:

$$M_1(B') \xrightarrow{B'\to\infty} \frac{1}{6B'^3};$$
$$M_2(B') \xrightarrow{B'\to\infty} \frac{1}{3B'^4}. \tag{6}$$

Therefore, the resulting limits for the $\mathscr{C}$-coefficient are given as:

$$\mathscr{C}(B') \xrightarrow{B'\to 0} 1 \quad (:= \mathscr{C}_{low}); \tag{7}$$
$$\mathscr{C}(B') \xrightarrow{B'\to\infty} \frac{11025}{5776}\frac{1}{B'^6} \quad (:= \mathscr{C}_{high} \approx 1.9B'^{-6}). \tag{8}$$

Hence, the coefficient $\mathscr{C}$ approaches unity in the case of weak fields ($B \ll B_{cr}$). In the strong field limit ($B \gg B_{cr}$), $\mathscr{C}$ scales like B'^{-6}. Therefore, as the δ-coefficient in the nondispersion limit (eq. 5) scales like $\mathscr{C}B'^6$, δ approaches constant values for high magnetic field strengths at fixed energies E_γ.
Full numerical calculations give results in agreement with these limiting cases.

Considering the asymptotic behaviour of $\mathscr{C}(B')$ and some exemplary values as given in table 1, one finds that $\mathscr{C}$ can be well approximated by 1 for $B' \leq 10^{-2}$ (i.e. $\Delta\mathscr{C}$ ($= |\mathscr{C}_{low}/\mathscr{C} - 1|$) < 0.01). The high field limit can be savely used for $B' \geq 10^3$ (i.e. $\Delta\mathscr{C}$ ($= |\mathscr{C}_{high}/\mathscr{C} - 1|$) < 0.01), which is already abve the field strength range of known astrophysical objects. These limits were used to plot $\mathscr{C}$ in figure 4 and in all the following calculations including the δ-coefficient for weak or strong field. There may be issues for which more accurate values for $\mathscr{C}$ have to be calculated. For this reason one can have a closer look at some specific values of $\mathscr{C}$ by looking at the exemplary values given in table 1 to estimate the accuracy of assuming the function as its asymptotes.

B'	$\mathscr{C}_{low}/\mathscr{C}$	$\mathscr{C}_{high}/\mathscr{C}$
0.00001	1.00000000001	1.9e36
0.0001	1.000000008	1.9e30
0.001	1.00000013	1.9e18
0.01	1.0013	1.9e12
0.1	1.13	2.15e6
1	30.2	57.6
10	9.6e5	1.9
100	5.6e11	1.08
1000	5.3e17	1.007
10000	5.2e23	1.00008
100000	5.2e29	1.000004

Table 1: Table of example values for the $\mathscr{C}$-coefficient. $\mathscr{C}_{high}$ refers to the limit for high values of B (see eq. 8)

The δ-coefficient as given by Eq. 2 is shown in figure 5 (A), where a fixed value for $\theta_{kB} = 90°$, i.e. $\vec{p} \perp \vec{B} := B_\perp$, has been assumed. The shaded part of the plot belongs to the region where vacuum dispersion effects have to be respected, i.e. where eq. 1 is not fulfilled. The power law behaviour of δ_{st} can be observed by considering the one dimensional plots shown in Fig 5 (B) and 5 (C). Therefore in each of them one parameter is kept as a fixed value.

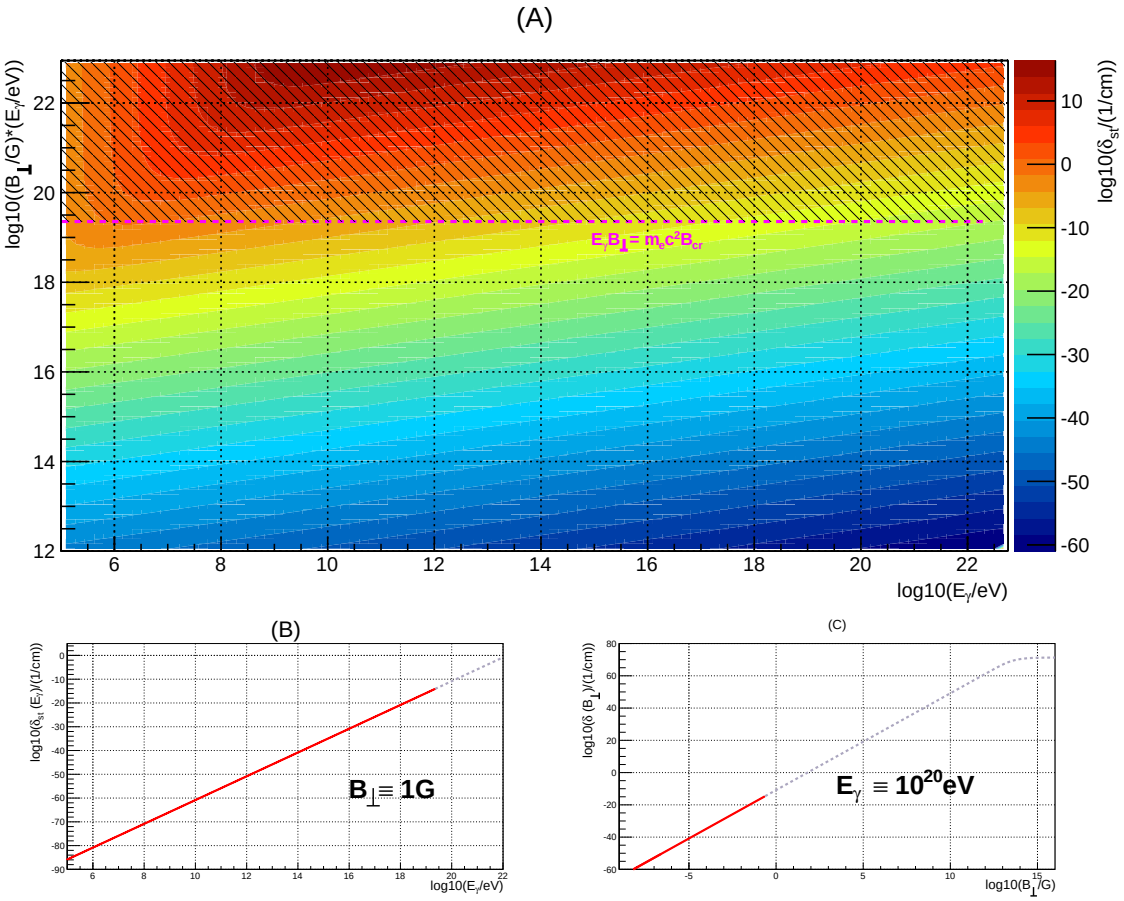

Figure 5: The attenuation coeffcient δ_{st} for photon splitting derived by Stoneham (Eq. 2 as a function of the parameters E_γ and $B_\perp$. The valid range of the formula for δ in (A) is the area below the dashed line, which marks the set of points, where the nondispersion condition (eq. 1) is fulfilled. In (A), the transverse magnetic field strength $B_\perp$, plotted on the vertical asixs, has been multiplied by E_γ in order to optimize the visibility of the significant region of the E_γ-$B_\perp$ phase space. The two plots below, show δ_{sk} for fixed values of $B_\perp = 1G$ (B) and $E_\gamma = 10^{20}$eV (C). The valid ranges here, also limited by the nondispersion relation (1), are illustrated by the continuous parts of the lines.

As suspected from looking at the formulas, the attenuation coefficient increases with increasing photon energy or transverse magnetic field until the nondispersion limit is reached. Due to the different powers of E_γ and $B_\perp$ in formula 2 and the nondispersion relation (Eq. 1), which is symmetric in E_γ and $B_\perp$, the dashed line is not parallel to the contours of δ. For this reason, the highest values in the valid range of δ are found for energies of $E_\gamma \approx 0.1$MeV - 1MeV in the

upper left corner of the E_γ-$B_\perp$ phase space just below the limiting line.

2.3 Comparison to the Photon Splitting Formula of Skobov

There is another formula in the literature for the attenuation coefficient of photon splitting. This formula, given for low magnetic field, i.e. $B \ll B_{cr}$ is claimed by Skobov [8] to be

$$\delta_{sk} = \frac{5}{3(144\pi)^2} \frac{\alpha_{em}^3}{\lambda\!\!\!^{-}} \frac{E_\gamma}{m_e c^2} \left(\frac{B_\perp}{B_{cr}}\right)^2 \tag{9}$$

where the same notation as in eq. 2 has been used. There are obvious differences comparing Eq. 9 to the formula as given by Stoneham (Eq. 2) mentioned above. Although both formulas claim the interaction being in third order in the fine structure constant α_{em}, the power law behaviour in the parameters E_γ and $B_\perp$ is obviously not the same. Furthermore, the range of validity is in both formulas, taking the low-B approximation formula of Stoneham, limited by the condition $B_\perp \ll B_{cr}$, but there is no cut in the valid range of the formula of Skobov at the point, where vacuum dispersion effects cannot be neglected. According to Stoneham [7], the formula given by Skobov is not correct. Here the quantitative differences between the two representations of the attenuation coefficient are analyzed to eventually specify a region in the phase space where the formulas give similar values and, as a result, determine the valid ranges for the, claimed to be incorrect, formula of Skobov. Therefore, the fraction $\delta_{sk}/\delta_{st}^{low}$ has been plotted in figure 6. Where δ_{st}^{low} denotes the attenuation coefficient according to stoneham in the low-B limit ($B \ll B_{cr}$). While the same low-B limit, represented by a dashed line in figure 6, can be used to restrict both formulas, the nondispersion limit is just valid for δ_{st}^{low}.

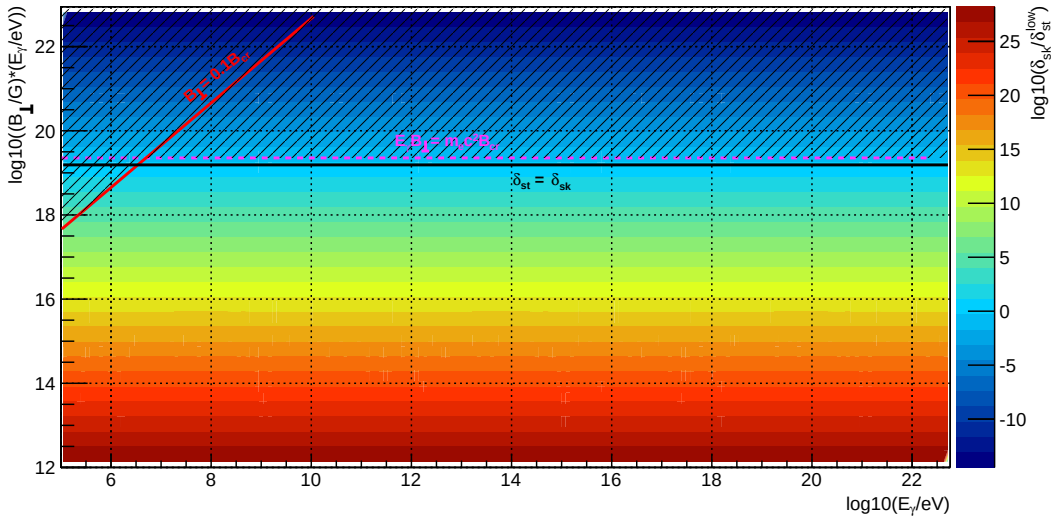

Figure 6: Comparison of the formulas for the magnetic photon splitting attenuation coefficient given by Skobov (Eq. 9) and Stoneham (Eq. 2). The magnetic field $B_\perp$, plotted on the vertical axis, has been multiplied by E_γ. The red line marks the region where $B = 0.1B_{cr}$ and denotes the limit for weak magnetic field in which both formulas are valid. At this limit, the deviation of the $\mathscr{C}$-coefficient (Eq. 1) to $\mathscr{C}_{low}$ (Eq. 7) is still very small, so that it was sufficient to plot just the weak field approximation od the attenuation coefficient δ_{st}^{low} given by Stoneham. The dashed line refers to equation 1 and marks the limit of nondispersion for δ_{st}^{low}. Note, that there is no nondispersion limit to the formula given by Skobov δ_{sk}. Furthermore, the contour line where the two versions of the attenuation coefficient are equal is drawn in black.

As one can see in figure 6 the formulas give almost the same results, considering only points very close to the line denoting the nondispersion limit. But the differences increase rapidly with the perpendicular distance to that line. This increase behaves like the difference of the exponents of the power laws, i.e. $\delta_{sk}/\delta_{st}^{low} \sim E_\gamma^{-4} B_\perp^{-4}$. This significantly different behaviour of the two formulas can be seen in figure 6. For this reason, the formula of Skobov, apparently the less reliable one, wont be used at all during the further procedure and the attenuation coefficient as given by Stonehem δ_{st} shall be called just δ from now on.

2.4 Comparison to Pair Production

Now, given that photon splitting is not the only possible attenuation process for electromagnetic radiation in ambient magnetic fields, the absolute probability for a photon to split not only depends on δ, but also on its probability to undergo pair production. For instance, if the attenuation coefficient of pair production is much higher than the one for splitting, splitting will not happen at all, even if very long propagation distances are considered because the photon will always do pair production long before there is an appropriate chance for it to split. For the interaction probabilities being linear processes in the attenuation coefficients, the proportion of the probability of the effects is equal to the proportion of the attenuation coefficients. For this reason it is necessary not to analyse photon splitting separately, but to compare its significance against pair production.

As pair production (figure 7) in the leading order is an electromagnetic interaction in the first order of the fine structure constant α_{em}, it is, compared to photon splitting (leading order $\sim \alpha_{em}^3$) more likely to be the dominant process. For this reason it is yet well treated by preshower programs. But, it is not so clear yet, whether the attenuation coefficient of photon splitting could become comparable to the one of pairproduction or even dominate it in some parts of the E_γ-$B_\perp$ phase space.

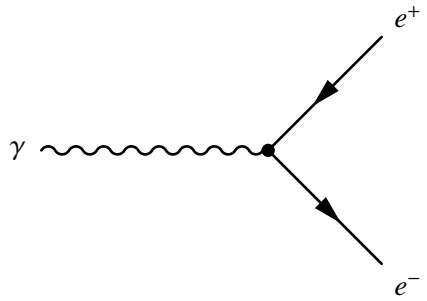

Figure 7: Feynman diagram for pair production (without the photon from the magnetic field)

The attenuation coefficient α for pair production as given by Erber [10] can be written as

$$\alpha(\chi) = 0.5\left(\frac{\alpha_{em} m_e c}{\hbar}\right)\left(\frac{B_\perp}{B_{cr}}\right) T(\chi) \tag{10}$$

with

$$T(\chi) \simeq 0.16\chi^{-1}K_{1/3}^2[2/3\chi], \tag{11}$$

$$\chi = \frac{E_\gamma}{m_e c^2}\frac{B_\perp}{B_{cr}} \tag{12}$$

and $K_{1/3}$ are the modified Bessel functions of order 1/3. Note, that for $\chi \lesssim 1$ the nondispersion relation, Eq. 1, is fulfilled.

The asymptotic behaviour of $T(\chi)$ can be calculated by using the limits of the modified Bessel function and is given by Erber [10]:

$$T(\chi) = \begin{cases} 0.46\exp(-\frac{4}{3\chi}) & ;\chi \ll 1 \\ 0.60\chi^{-1/3} & ;\chi \gg 1 \end{cases} \tag{13}$$

Where the limiting case $\chi \gg 1$ refers to regions of high dispersion. Therefore this limit is not relevant for the comparison to photon splitting, because the used formula (Eq. 2) is only valid for negligible dispersion.

By plugging these limits into α one can conclude the behaviour of the attenuation coefficient for high values of $B_\perp$ and E_γ:

$$\alpha \sim B_\perp^{\frac{2}{3}} E_\gamma^{-\frac{1}{3}} \qquad ; E_\gamma B_\perp \gg m_e c^2 B_{cr} \tag{14}$$

and for low values the function has a decrease like

$$\alpha \sim B_\perp \exp(-1/(E_\gamma B_\perp)) \qquad ; E_\gamma B_\perp \ll m_e c^2 B_{cr} \tag{15}$$

The numerical solution for $\alpha(E_\gamma, B_\perp)$ is shown in figure 8. For plotting this function, α has been approximated with the limit of $T(\chi)$ for small values of χ as $\chi < 0.1$. This limit is also used in PRESHOWER when calculating the attenuation coefficient [1].

[1] In fact, there are two limits set in PRESHOWER during the calculation of α. The first one is the one mentioned above at $\chi = 0.1$. The second one is an approximation of the modified Bessel function itself at $\kappa\left(= \frac{2}{3\chi}\right) \geq 10^2$ where κ is the argument of the Bessel function. The second limit has been implemented because of the difficulty to calculate values of the Bessel function for high arguments by using the default numerical procedure. But this limit is never reached in the program because of the previous approximation of $T(\chi)$. That makes the second limit redundant.

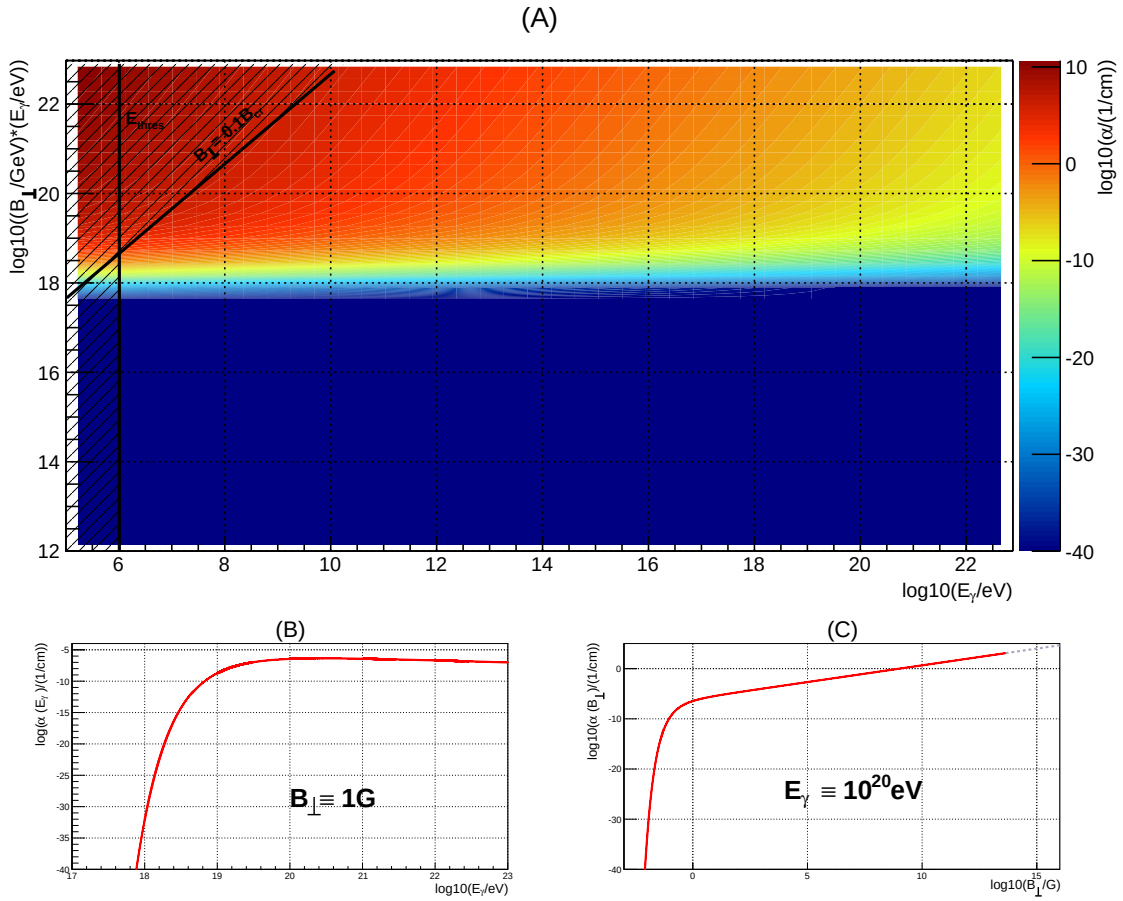

Figure 8: In (A), the attenuation-coeffcient for pair production α is shown as a function of the parameters E_γ and $B_\perp$. Small values for $\alpha(< 10^{-40})$ are drawn in dark blue and are not distinguished furthermore. The plots (B) and (C) refer to fixed values of $B_\perp = 1$G (B) and $E_\gamma = 10^{20}$eV (C). The black line in (A) as well as the dotted part of the line in (C) refer to the low-field condition $B = 0.1B_{cr}$. Note, that there is also a threshold energy E_{thres} for pair production at $2m_e ec^2 \approx 1$MeV. Below this energy, a photon cannot undergo pair production due to energy conservation.

As one can see in figure 8, the α-ceofficient is a monotonically increasing function in the magnetic field strength, but has a maximum in the photon energy, which is a basically different behaviour from the attenuation coefficient of photon splitting. In the example of figure 8 (B) this maximum can be located at about $10^{22.5}$eV. Due to the highly different behaviour in the limits compared to δ (discussed for α in equations 14 and 15 and for δ by plugging equation 8 into equation 2) which can be qualitatively considered by looking at figures 5 and 8 one can already conclude that there are some parts of the phase space, where the probability of photon splitting exceeds the probability of pair production. These parts are most likely in the lower left corner of the phase space, where the power law behaviour of δ (figure 5) dominates the decrease of α (figure 8). Also for high photon energies one would expect photon splitting to be significant against pair production at some point because of the decreasing values of α with rising energy.
To quantify the above considerations, the proportion of δ to α has been calculated numerically and drawn as a color-plot in the phase space spanned by E_γ and $B_\perp$ in figure 9. The green lines indicate the locations where $\delta = 0.01\alpha$. The lower green line and the nondispersion limit margin the area where splitting definitely can be estimated to be a significant process compared to pair production. That means in the area between these lines photons are not likely to undergo splitting because pair production is by far the most dominant process. Furthermore, for simplicity, the attenuation coefficient of photon splitting has been drawn in the low-B limit, which is marked by the black line at $B = 0.1B_{cr}$. Note, that the validity of δ is still limited by the nondispersion relation (1) which allows no conclusive statements for values above this limit.

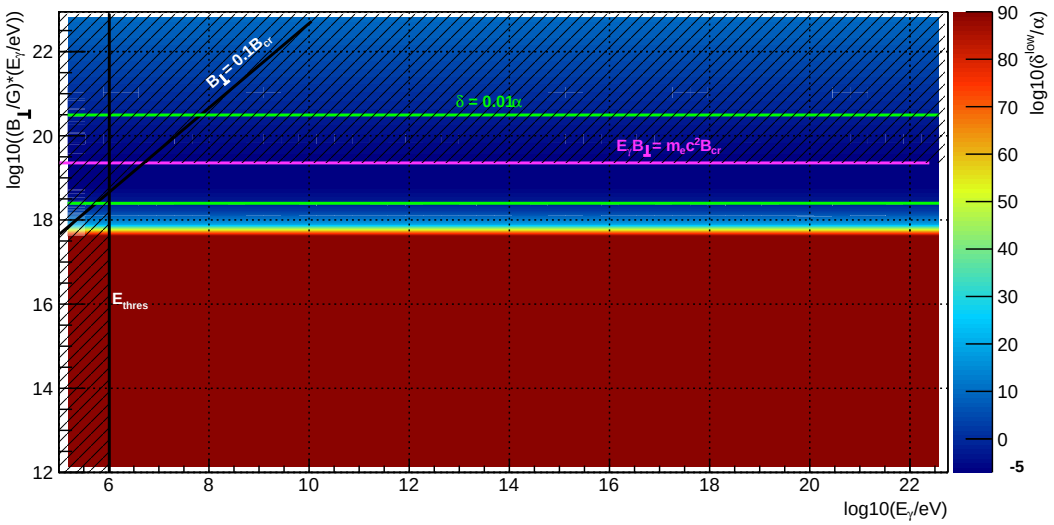

Figure 9: The proportion of the attenuation coefficient of photon-splitting to the one of pair production. As before, the range of validity of the δ-coefficient is illustrated by the two lines referring to the nondispersion limit, the low field limit (which also applies to α) and the threshold energy E_{thres} for pair production. The two green lines delimit the regions where $\delta_{st} \leq 0.01\alpha$. That means, that δ is less than 0.01α only in the space between the two lines. Regions at the bottom of the plt drawn in red refer to proportions higher then 10^{90}. Although photon-splitting is the dominant process in these regions, they are of no much interest because the absolute value of both processes is here negligibly small.

Taking account of the nondispersion limit (1) which is marked by the pink line in figure 9 one still finds a part of the valid phase space, where photon splitting can absolutely be excluded to be a relevant process because of the fact of being suppressed by at least two orders of magnitude compared to pair production. This part is the region between the lower line of the 0.01-mark and the nondispersion limit.

Now, the question arises, whether there are any physical conditions, for which the photon splitting probability reaches a significant level compared to the probability of pair production and, concurrently, the total splitting probability is not negligibly small. Only under such circumstances the photon splitting process is worth being taken into account.

2.5 The probability of Photon Splitting in Different Circumstances

The intention of analysing the attenuation coefficient in the first place instead of the splitting probability itself is its independence of the propagation length. Hence, the attenuation coefficient just depends on the photon energy and the transverse magnetic field but not on the distance a photon travels under these conditions. The total splitting probability within a propagation length x in a static ambient field is related to the attenuation coefficient δ like

$$P_{sp}(x) = 1 - e^{-\delta x}. \tag{16}$$

In the case of small steps Δx the splitting probability is proportional to x where the constant of proportionality is the attenuation coefficient δ, i.e. $P_{sp}(\Delta x) \approx \delta \Delta x$. This can mathematically be achieved by applying the Taylor expansion for the exponential function in equation 16 and neglecting all higher orders of δ. It is therefore necessary to analyse not just the attenuation coefficient itself, which can be identified as the splitting probability in an infinitesimal step of the path, but the total splitting probability along the whole path. For example, there would be no need to deal with photon splitting in simulations when the splitting probability under the considered circumstances is about 10^{-3} even if the attenuation coefficient for photon splitting was much higher than the one for pair production under these circumstances. In this case there would most likely be no interaction at all due to the low flux of high energy photons.

To get an overview of the total probability of a photon to undergo splitting it is convenient to assume a constant transverse magnetic field along the whole trajectory of the photon. This gives a constant attenuation coefficient for the whole propagation and therefore, the splitting probability obeys an exponential attenuation law (Eq. 16)

Furthermore it is reasonable to restrict the analysis in this case to realistic conditions in terms of diameter and magnetic field strength. For this reason, some representative astrophysical objects were taken from figure 10 (see [11]) to obtain the realistic range for the magnetic fields and an average diameter. This diameter was assumed to be the propagation distance x.

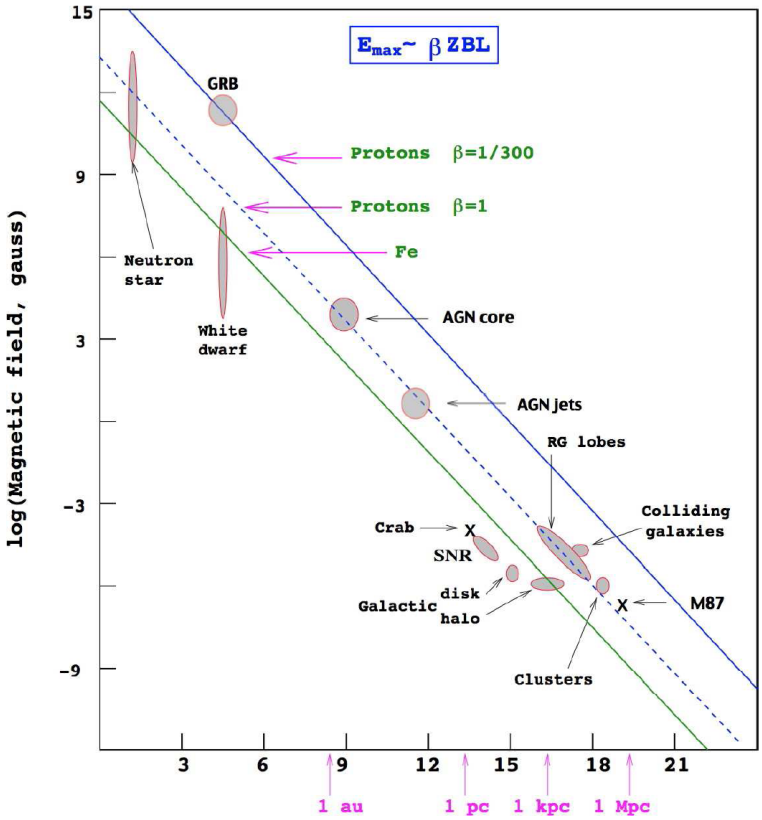

Figure 10: The sizes and characteristic magnetic field strenghts of selected astrophysical objects. The lines in the plot are related to assumptions about possible acceleration mechanisms, which are not further discussed in this work. The diagram was taken from [11].

To get a first view of the splitting probability along different propagation lengths some exemplary objects were considered, which are equally distributed among figure 10. The chosen objects are, a neutron star, a gamma ray burst (GRB), the core of an active galactic nucleus (AGN) and the lobes of a radio galaxy. In addition to that, the Earth magnetosphere and the whole Universe itself have been studied. The splitting probability has been analysed in terms of the dimensions of these 6 astrophysical objects as seen in figure 11. To get an overall view of a scenario, in each case the wide range of the E_γ-$B_\perp$ phase space has been plotted, and the intrinsic range of magnetic field is marked by the dashed lines. For simplicity, the attenuation coefficient in the low-B limit as well as the nondispersion limit were applied to calculate the splitting probability.

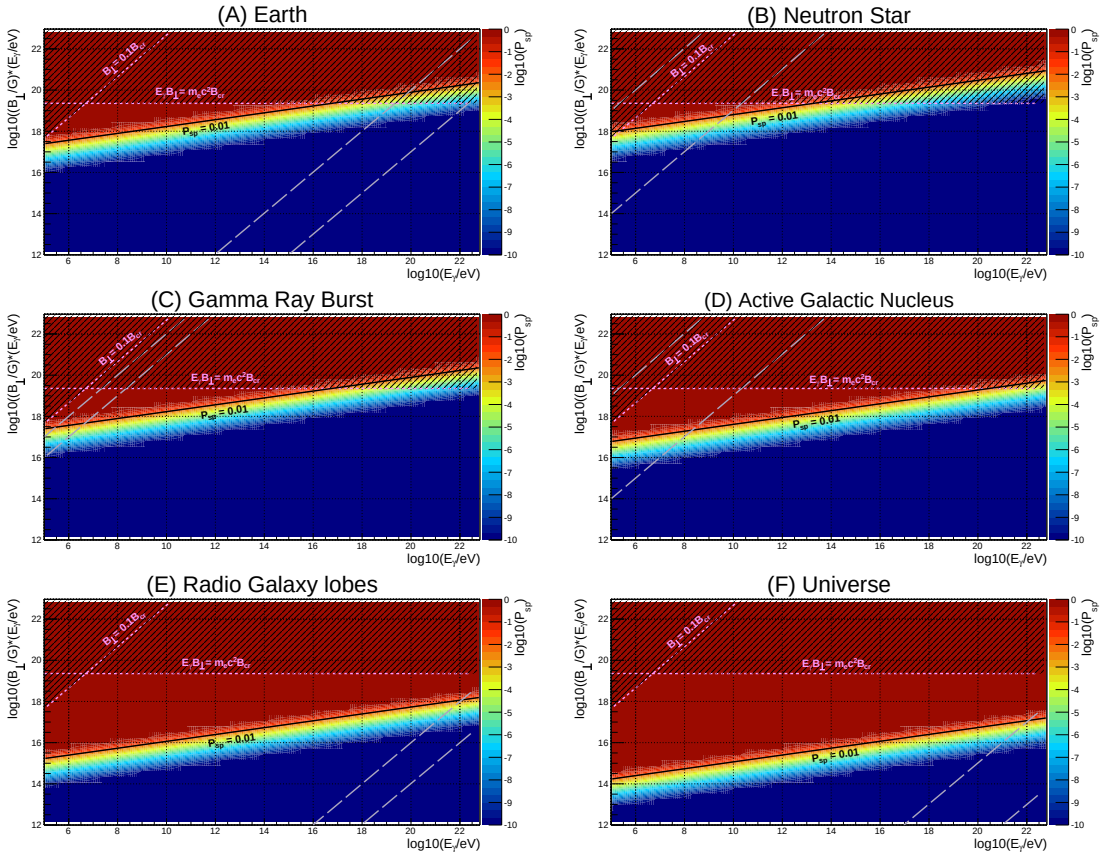

Figure 11: Assuming a photon travelling a distance as long as the diameter of the Earth magnetosphere, a neutron star, a gamma ray burst, the core of an active galactic nucleus, the lobes of a radio galaxy and the whole Universe in a constant transverse magnetic field, the total splitting probability is drawn as a function of the ehotons energy and the constant transverse magnetic field.

The two dotted (pink) lines in the plots refer to the nondispersion limit (eq. 1), and the low-field limit $B_\perp = 0.1B_{cr} \ll B_{cr}$ (witch both limit the range of validity of the used approximation of the attenuation coefficient). The contours where the splitting probabilities $P_{sp} = 0.01$ are marked by the continuous (black) lines. The dashed (grey) lines refer to constant B-values and set the limits to the range of magnetic field strengths characteristic for these specific objects.

The values for the average diameters and the ranges for the magnetic fields for the neutron star, the GRB, the AGN core and the RG lobes were estimated by considering the values from figure 10: ∅ (B) neutron star: $\sim$ 10km; ∅ (D) AGN core: $\sim$ 1au; ∅ (C) GRB: $\sim 3 \cdot 10^4$km; ∅ (E) RG lobes: $\sim$ 10kpc; The typical propagation length in the Earth magnetic field was taken from the PRESHOWER program and the diameter of the Universe has been obtained by current estimations [14]: ∅ (A) Earth magnetic field: $\sim 3 \cdot 10^4$km; ∅ (F) Universe: $\sim$ 28Gpc

It is very important to analyse the significance of photon splitting in the Earth conditions in order to improve the PRESHOWER simulations if necessary. The diameter of the Earth magnetosphere has been assumed to be 30.000 km, which is the particle propagation distance in PRESHOWER begins. For the transverse magnetic field a range from 10^{-3}G to 1G has been considered, which covers the values typical for the geomagnetic field. By having a look at figure 11 (A) it turns out that photon splitting in Earth conditions is more likely to occur at the upper range of the γ-energy spectrum for fixed values of B_γ (lines parallel to the dashed grey ones). That is because of the upper limit of $B_\perp = 1G$ which prevents photons at lower energies to undergo splitting. The splitting probability in Earth conditions has been redrawn and zoomed in for the interesting ranges in figure 12.

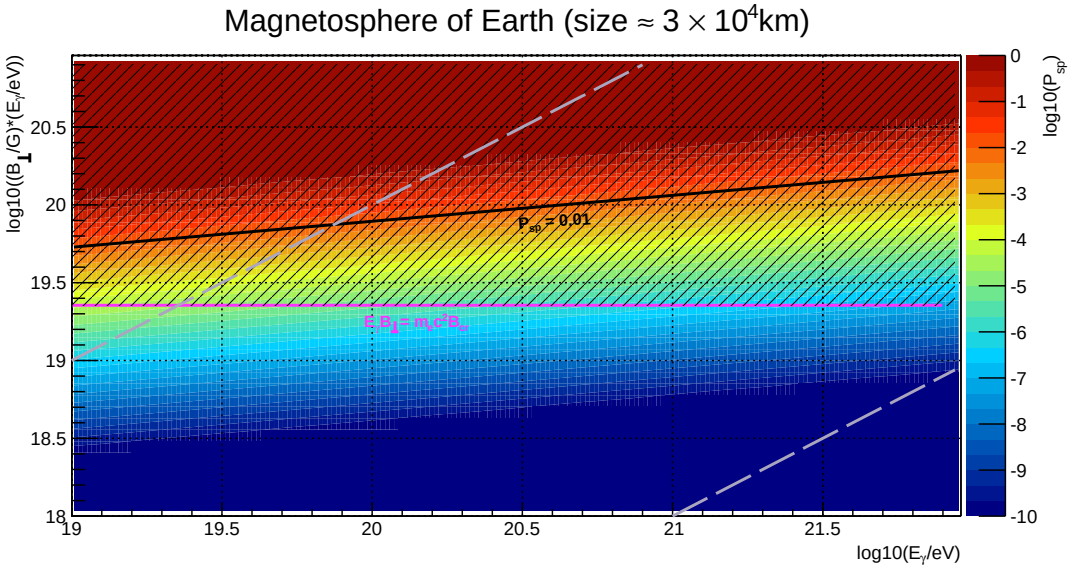

Figure 12: The figure shows the total splitting probability in the case of the Earth (see upper left plot of figure 11) in the area of the phase space which would be relevant for UHE photons in Earths conditions

Considering figure 12 one realizes, that in the whole region in the E_γ-$B_\perp$ plane, where P_{sp} is higher than 0.01 the nondispersion limit does not allow a valid approximation for δ. For this

reason, one cannot exclude photon splitting to happen in the area of relevant vacuum dispersion, but there is definitely no use in implementing the formula for photon splitting, as given in the nondispersion limit, in the PRESHOWER calculations. Furthermore one can say, that analysing photon splitting in the area of significant dispersion is just necessary for investigating photons at energies above $\sim 10^{19.5}$eV. For energies below that value photon splitting in Earth conditions is very unlikely to happen.

In figure 11 (B) the circumstances within the vicinity of a neutron star are displayed. According to figure 10, a travelling distance of 10km and a range of the magnetic field strength from 10^9G to 10^{14}G (magnetic field strengths vary within different neutron stars) were assumed. As one can see, there is actually an area, where the splitting probability is above 0.01 and the nondispersion approximation can be applied. To cover all the range of magnetic field values typical for a neutron star, the splitting probability was calculated again without the low-B limit. The splitting probability for of a neutron star without the low-B limit zoomed into the area of interest is shown in figure 13. The splitting probability has been calculated here also for lower values of E_γ than in figure 11 (B) to see better the increased significance of photon splitting at lower energies.

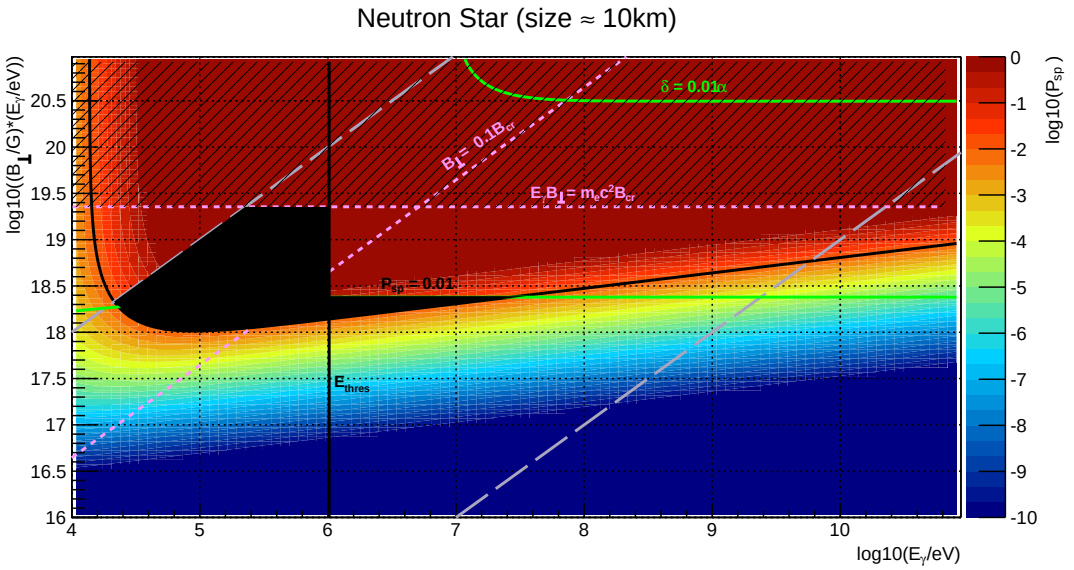

Figure 13: The total splitting probability in case of a neutron star recalculated using the generalized formula for δ at higher values of B. The limit, where $P_{sp} = 0.01$ is marked by the black line. The green lines refer to those from figure 9 and mark the area where $\delta_{st} = 0.01\alpha$. The area between these lines refers to the regions where δ is less then 0.01 of α. The interesting region, where the photon splitting coefficient is significant compared to the pair production one as well as the total splitting probability P_{sp} are not negligibly small is marked by the black filled area. Note that for photon energies below E_{thres} there is no pair production at all and therefore photon splitting is not in competition with pair production. Heere δ was calculated using the formula without the low-B limit (Eq. 2), while the α-coefficient as given by Erber can be obtained only for $B < 0.1B_{cr}$. Thats why for the proportion of both coefficients the low-B limit has been applied.

Considering figure 13 one sees a region in the valid range of the used formulas, where a very good chance for a photon exists to undergo splitting. In the plot that region is bounded by the lines according to the nondisperison limit, the mark for the 0.01 splitting probability and the upper und the lower limits for the magnetic field of a neutron star. Hence in most part of that region the splitting probability is close to 1. That means, that photon splitting is almost guaranteed to occur unless it is not suppressed by pair production in this part of the phase space. To analyse wheather this is the case, the contour lines where the proportion of the attenuation coefficients of splitting to pair production is equal 0.01 are shown as green lines in figure 13. For photon energies below the threshold energy E_{thres} there is no copetition at all between photon splitting and pairproduction because photons can not undergo pairproduction at energies $E_\gamma < E_{thres}$ due

to energetic reasons. After comparing the relative interaction probabilities there is still a small region left in the phase space where photon splitting could be a significant effect. This region is marked by the black filled area.

Also for typical GRB (Fig. 11 (C)) and AGN cores (Fig. 11 (D)) some phase space areas exist where the probability of photon splitting is at a significant level within the nondispersion phase space region.
Finally, the splitting propabilities for the scales and the magnetic conditions of the lobes of a Radio Galaxy and of the entire Universe itself are shown in figures 11 (E) and (F). For the Universe case, the magnetic field strengths in the intergalactic medium values in the range of 10^{-9}G to 10^{-5}G were assumed. In this case, as well as in the case of a radio galaxy, the splitting probabilities exceed the 0.01 mark just at photon energies somewhere above $\sim 10^{22}$eV. Such photons can not be excluded to exist, but for the reason that there is no evidence for particles at these energies yet, they aren't considered any further at this point.

3 Conclusions

3.1 Summary of Results

Although there is no evidence yet, that the photon splitting effect can completely be excluded to be significant in terms of preshower propagation, one can conclude, that it can be excluded under nondispersion conditions. Therefore it is definitely not necessary to take the attenuation coefficient as given in eq. 2 into account when simulating preshower developments. Furthermore, considering photons at energies $< 10^{19.5}$eV photon splitting has proven to be irrelevant at all within preshowers for its probability to occur for a single photon is less then 0.01.
Looking at a wider range and considering further conditions in which UHE photons are likely to occur, one realizes, that there are some astrophysical objects at which photon splitting indeed could be a relevant process as in the cases of Gamma Ray Bursts and the cores of AGNs. In the case of an UHE photon being radiated from a neutron star or passing nearby, it has been shown explicitly, that, at some parts of the E_γ-$B_\perp$ phase space, photon splitting reaches a significant

level not just in terms of separated splitting probability but also in comparison to pair production which is a competing process to splitting. This part has been found somewhere in the range between $E_\gamma = 10^{4.4}...10^{7.5}$eV and $B_\perp = 10^{11}...10^{14}$G (see the black area in Fig. 13).
It turned out, that the photon splitting effect in the vicinity of neutron stars with maximum magnetic fields up to 10^{14}G can be completely calculated with the formula in the nondisperion approximation (Eq. 5) for photon energies below $10^{5.4}$eV. If ones intends to use that approximation for higher energies, it would be possible only for weaker magnetic fields.

3.2 Prospects

Although the photon splitting effect can be excluded in the nondispersion Earth conditions, there is a large area in the phase space where vacuum dispersion is not a negligible effect and formula 2 can not be used. In this region a more general formula which is valid for any values of E_γ and $B_\perp$ should be applied. Such a formula has been investigated by Stoneham [7]. This formula, however, is very complicated and its application for numerical calculations is highly untrivial, if possible at all. The analysis shown here have proven, that it is necessary to investigate the application of this general formula more closely. Especially in the case of ultra high energy photons, vacuum dispersion effects become highly significant even at low magnetic fields like the geomagnetic field. Also in wide ranges of the E_γ-$B_\perp$ phase spaces for neutron stars conditions as well as for the cases of GRBs, AGNs and RG lobes, vacuum dispersion effects have to be taken into account to perform complete propagation simulations.
One could cross-check the presented results with the ones existing in literature. For instance, Harding and Baring [9] calculated the absolute probability for photon splitting by integrating the attenuation coefficient over a trajectory starting perpendicular to the surface of a neutron star and taking the Schwarzschild metrics into account. The same could be done with PRESHOWER. For this purpose, one needs to replace the geomagnetic field model used by PRESHOWER with a dipole model of parameters typical for a neutron star and introduce the Schwarzschild metric in the calculations.
In addition to the previously considered circumstances, one could analyze the photon splitting effect taking into account plasma physic. Although the propagation lengths in artificial plasma

beams are relatively small compared to the astrophysical dimensions considered above, the magnetic field strengths and the high particle energies inside plasma could make photon splitting a significant process.

References

[1] M. Risse, P. Homola, *Modern Physics Letters A* **22**, 11 (2007).

[2] M. Risse et al., *Astroparticle Physics* **21** (2004).

[3] P. Homola et al., *Computer Physics Communication* **173** (2005).

[4] http://www.jirka.org/genius.html

[5] http://gmplib.org/

[6] http://root.cern.ch/drupal/

[7] R. J. Stoneham, *J. Phys. A: Math. Gen.,* **12**, 11 (1979).

[8] Skobov, V. G., Zh. Eksperim, i Teor. Fiz, **35**, 1315 (1958).

[9] A. Harding, M. Baring, P. Gonthier, *The Astroph. Journal* **476** (1997).

[10] T. Erber, *Rev. Mod. Phys.,* **38**, 4 (1966).

[11] A. Letessier-Selvon, T. Stanev, *Rev. Mod. Phys.,* **83** (2011).

[12] M. Baring, *Astron. Astrophys.* **249** (1991).

[13] U. Sigl, P. Bhattacharjee, *Phys. Rep.* **327** (2000).

[14] J. R. Gott et al., *The Astroph. Journal* **624** (2), 463 (2005).

[15] K. Greisen, *Phys. Rev. Lett.* **16**, 748 (1966).

[16] G. T. Zatsepin and V. A. Kuzmin, *JETP Lett.* **4**, 78 (1966).

[17] Pierre Auger Collab., *Nucl. Instr. Meth. A* **523**, 50 (2004).

[18] D. J. Bird et al., *Astrophys. J.* **441**, 144 (1995).

[19] M. Fukushima et al., *Prog. Theor. Phys. Suppl.* **151**, 206 (2003).

[20] D. Heck, J. Knapp, J.N. Capdevielle, G. Schatz, T. Thouw, Report FZKA 6019, Forschungszentrum Karlsruhe, available at http://www.ik. fzk.de/ heck/corsika/, 1998.

[21] D. Heck, J. Knapp, available at http://www.ik.fzk.de/ heck/corsika/userguide/corsika_tech.html.

[22] S. J. Sciutto, astro-ph/9911331.